

Mix-mode fracture of microplates

Pham Hong Cong^{1,*}, Do Van Thom^{2,*}, Doan Hong Duc³, Phung Van Minh²,
Pham Duc Nhat³, Dong Xuan Truong⁴

¹Centre for Informatics and Computing, Vietnam Academy of Science and Technology,
18 Hoang Quoc Viet, Cau Giay, Ha Noi, Viet Nam

²Le Quy Don Technical University, 236 Hoang Quoc Viet, Cau Giay, Ha Noi, Viet Nam

³Hanoi University of Science and Technology, 1 Dai Co Viet, Hai Ba Trung, Ha Noi, Viet Nam

⁴University of Engineering and Technology, VNU, 144 Xuan Thuy, Cau Giay, Ha Noi, Viet Nam

*Emails: phcong@cic.vast.vn, thom.dovan@lqdtu.edu.vn

Received: 27 March 2023; Accepted for publication: 19 April 2023

Abstract. This paper studies the crack propagation of microplates in mix-mode based on a modified couple stress theory (MCST) and the phase-field method. Compared to the stress couple hypothesis, the MCST contains many novel aspects, most notably the symmetry of the couple stress tensor and the involvement of a single internal length scale parameter. These features make the modified couple stress theory easier to use. The formulas are established based on the finite element method (FEM). When calculated using the MCST versus classical theory (regardless of size effect), the calculation results unmistakably demonstrate the differences in the mechanical characteristics of the system during the crack development. The difference is demonstrated by specific examples, with clear explanations and many physical meanings. This work will be helpful for researchers studying the process of **microstructural** fracture formation.

Keywords: Size-effect, microplates, couple stress, crack, phase-field.

Classification numbers: 5.4.2, 5.4.5

1. INTRODUCTION

Nano- and micro-sized materials and structures are now widely used in modern engineering. In particular, the problem of studying the mechanical behavior of these structures plays an important role in the design and manufacturing processes. Scientists have developed many different theories and achieved much in solving these problems. In 1994, Fleck *et al.* [1] introduced a theoretical and experimental study on strain gradient plasticity. Using dislocation theory, a strain gradient theory of rate-independent plasticity was invoked. The build-up of both randomly stored and geometrically essential dislocations was believed to cause hardening. Stölken and Evans [2] carried out a microbend test method for measuring the plasticity length scale. Stelmashenko *et al.* [3] explored the microindentation on W and Mo oriented single crystals. Nix and Gao [4] investigated the indentation size effects in crystalline materials using

the law of strain gradient plasticity. Poole and co-workers [5] examined the micro-hardness of annealed and work-hardened copper polycrystals. Lam *et al.* [6] carried out an experimental and theoretical study of strain gradient elasticity. Some other typical and important works can also be found in [7-14].

Leppington and Atkinson [15] introduced some calculations of the energy release rate G for cracks in micropolar and couple-stress elastic media. Then, they studied the effect of a couple stresses on the tip of a crack [16]. Daneshmehr and Homayounfard [17] discussed the study of size-dependent energy release rate formulation of notched beams based on the MCST. Georgiadis and Gourgiotis [18] applied an approach based on distributed dislocations and disclinations for crack problems in couple-stress elasticity. Georgiadis and Baxevanakis [19] developed a displacement-based formulation for interaction problems between cracks and dislocation dipoles in couple-stress elasticity. Placidi *et al.* [20] formulated a linear elastic second gradient isotropic two-dimensional continuum model accounting for irreversible damage. Barchiesi and Placidi [21] carried out the energy method for brittle fracture in strain-gradient modeling. Suh and colleagues [22] developed a phase field model for cohesive fracture in micropolar continua. Thom *et al.* [23] presented the new numerical results of the vibration behavior of cracked FG plates based on phase-field theory and the FEM.

Using the phase-field hypothesis to simulate cracks, the current work proposes a strategy for addressing the crack model problem of modified couple-stress elasticity. As shown by research [25 - 31, 41 - 46], this strategy has a number of advantages for managing fracture problems. This is a fascinating research topic since it illustrates the difference in crack formation between ignoring the size-effect and considering the modified pair stress theory. In addition, this is the first research to illustrate the influence of macro and micro parts on the formation of cracks. The results of this work illuminate a number of fascinating physical properties of micromaterial fractures. This paper's structure is broken into five sections. Section 2 provides a concise overview of the MCST for 2D issues. In Section 3, the phase-field hypothesis and MCST-derived finite element formulations for the growing fracture problem are presented. The fourth section shows and analyzes the numerical results. In concluding section 5, some significant discoveries are highlighted.

2. FORMULATION

Based on the standard pair stress hypothesis [13, 14], the MSCT [32] takes into account the equilibrium of the moments of couples, resulting in a symmetric couple stress tensor. Thus, strain and just the symmetric component of the rotation gradient tensor contribute to the power, and the amount of material length-scale factors is reduced to one. The modified pair stress theory has also been empirically [6] and computationally [33] confirmed. Moreover, it has been acknowledged by a large number of researchers.

For the sake of completeness, the theory is briefly stated below. Both the rotation vector β_k and the strain tensor α_{ij} are connected to the vector u_i .

$$\alpha_{ij} = (u_{i,j} + u_{j,i}) / 2; \quad \beta_k = e_{kij} u_{j,i} / 2 \quad (1)$$

in which e_{kij} is Levi-Civita symbol; u_i and u_j are displacements along the x and y axes. the curvature tensor (χ_{ij}) is:

$$\chi_{ij} = (\beta_{i,j} + \beta_{j,i}) / 2 \quad (2)$$

The density of energy $\tilde{\Theta}$ can be estimated as [21]:

$$\tilde{\Theta} = \tilde{\Theta}(\alpha_{ij}, \chi_{ij}) = \frac{1}{2} \zeta_{ij} \alpha_{ij} + \frac{1}{2} \kappa_{ij} \chi_{ij} \quad (3)$$

in which ζ_{ij} is Cauchy stress tensor and κ_{ij} is the deviatoric component as follows:

$$\zeta_{ij} = \frac{\partial \tilde{\Theta}}{\partial \varepsilon_{ij}} = D_{ijkl} \alpha_{kl}; \quad \kappa_{ij} = \frac{\partial \tilde{\Theta}}{\partial \chi_{ij}} = 2\mu l^2 \chi_{ij} \quad (4)$$

in which μ is shear modulus, D_{ijkl} represents the elasticity tensor, and l is the length-scale parameter.

All components of the potential energy are represented by the following equation:

$$\Psi = \frac{1}{2} \int_{\Omega} \zeta_{ij} \alpha_{ij} d\Omega + \frac{1}{2} \int_{\Omega} \kappa_{ij} \chi_{ij} d\Omega - \int_{\Omega} f_i u_i d\Omega - \int_{\Omega} y_i \beta_i d\Omega - \int_{\Gamma^t} t_i u_i dS - \int_{\Gamma^q} q_i \beta_i dS \quad (5)$$

By applying the variational law $\delta\Psi = 0$, we can derive the equilibrium equation and initial provisos:

$$\begin{aligned} \zeta_{ji,j} + e_{jki} (\kappa_{lj,lk} + y_{k,j}) / 2 + f_i &= 0 \text{ in } \Omega; \\ n_j \zeta_{ji} + e_{jki} n_j (\kappa_{lk,l} - (\kappa_{pq} n_p n_q)_{,k} + y_k) / 2 &= \bar{t}_i - e_{ijk} n_j (\bar{q}_l n_l)_{,k} / 2 \text{ or } u_i = \bar{u}_i \\ \kappa_{ij} n_j - \kappa_{pq} n_p n_q n_i &= \bar{q}_i - \bar{q}_l n_l n_i \text{ or } \beta_i = \bar{\beta}_i \text{ on } \Gamma \end{aligned} \quad (6)$$

in which \bar{t}_i , \bar{q}_i , \bar{u}_i , and $\bar{\beta}_i$ are the boundary values that have been given.

The parameter θ_i was introduced by Garg *et al.* [34], which is distinct from β_i . Hence, with the parameter θ_i , one gets:

$$\kappa_{ij} = 2\mu l^2 \chi_{ij}; \quad \chi_{ij} = (\theta_{i,j} + \theta_{j,i}) / 2 \quad (7)$$

It is set $\theta_i = \beta_i$ due to the intrinsic differences between β_i and θ_i . To account for this disparity, the Lagrange parameter λ_i must be included.

When dealing with circumstances that only involve two dimensions, the total potential energy (using Lagrange multipliers) may be determined as:

$$\begin{aligned} \Psi^L &= \frac{1}{2} \int_{\Omega} \alpha_{ij} D_{ijkl} \alpha_{kl} d\Omega + \int_{\Omega} \kappa_{ij} \chi_{ij} d\Omega + \int_{\Omega} \lambda_i (\theta_i - \beta_i) d\Omega \\ &- \int_{\Omega} f_i u_i d\Omega - \int_{\Omega} y_i \beta_i d\Omega - \int_{\Gamma^t} t_i u_i dS - \int_{\Gamma^q} q_i \beta_i dS \end{aligned} \quad (8)$$

According to [17, 26], the constraint term on the surface $\int_{\Gamma} \lambda_i (\theta_i - \beta_i) d\Gamma$ may become zero if the mesh is refined further.

The expression that arises from using the variational idea is as follows:

$$\begin{aligned} \delta\Psi^L &= \int_{\Omega} \alpha_{ij} D_{ijkl} \delta\alpha_{ijkl} d\Omega + \int_{\Omega} \kappa_{ij} \delta\chi_{ij} d\Omega + \int_{\Omega} \delta\lambda_i (\theta_i - \omega_i) d\Omega + \int_{\Omega} \lambda_i (\delta\theta_i - \delta\beta_i) d\Omega \\ &- \int_{\Omega} f_i \delta u_i d\Omega - \int_{\Omega} y_i \delta\beta_i d\Omega - \int_{\Gamma^t} t_i \delta u_i dS - \int_{\Gamma^q} q_i \delta\beta_i dS \end{aligned} \quad (9)$$

3. PHASE-FIELD FORMULATION

Marigo and Francfort [35] presented the application of the phase-field hypothesis to fracture problems, which was later acquired by Miehe *et al.* [36], [37] for fracture issues. With a few small modifications, we use this continuous phase-field model to investigate fractures. The total energy of the fracture model is indicated by:

$$\begin{aligned} \tilde{U}(\Psi^L, s) = & \frac{1}{2} \int_{\Omega} s^2 \alpha_{ijij} D_{ijkl} \alpha_{ijkl} d\Omega + \frac{1}{2} \int_{\Omega} s^2 \kappa_{ij} \chi_{ij} d\Omega + \int_{\Omega} \lambda_i (\theta_i - \beta_i) d\Omega \\ & - \int_{\Omega} f_i u_i d\Omega - \int_{\Omega} y_i \beta_i d\Omega - \int_{\Gamma^t} t_i u_i dS - \int_{\Gamma^q} q_i \beta_i dS \\ & + \int_{\Omega} K_c \left(\frac{(1-s^2)^2}{4l_0} + l_0 |\nabla s|^2 \right) d\Omega = U_1 + U_2 + U_{crack} - U_{force} \end{aligned} \quad (10)$$

where

$$\begin{aligned} U_1 = & \frac{1}{2} \int_{\Omega} s^2 \alpha_{ijij} D_{ijkl} \alpha_{ijkl} d\Omega, U_2 = \frac{1}{2} \int_{\Omega} s^2 \kappa_{ij} \chi_{ij} d\Omega, U_{crack} = \int_{\Omega} K_c \left(\frac{(1-s^2)^2}{4l_0} + l_0 |\nabla s|^2 \right) d\Omega \\ U_{force} = & \int_{\Omega} f_i u_i d\Omega + \int_{\Omega} y_i \beta_i d\Omega + \int_{\Gamma^t} t_i u_i dS + \int_{\Gamma^q} q_i \beta_i dS - \int_{\Omega} \lambda_i (\theta_i - \beta_i) d\Omega \end{aligned} \quad (11)$$

where U_1 and U_2 represent microstrain energies, U_{crack} represents surface/crack energy, l_0 represents the length-scale characteristic of the crack, and K_c represents the rate at which the critical strain energy is set free. The parameter s has a value from 0 to 1, which distinguishes between fragmented and unbroken material ($s = 0$ and $s = 1$). Several unique degrading roles have been hypothesized in the literature and are thoroughly explored in [18], [38], [41-46].

Yet, the primary purpose of this work is to analyze crack propagation in mix-mode to obtain deeper knowledge. As a result, as mentioned in Eq. (10), isotropic strain energy degradation is applied in this study.

By using the virtual work principle, the weak form is:

$$\begin{aligned} & \int_{\Omega} s^2 \alpha_{ijij} D_{ijkl} \delta \alpha_{ijkl} d\Omega + \int_{\Omega} s^2 \kappa_{ij} \delta \chi_{ij} d\Omega \\ & = \int_{\Omega} f \delta_i u_i d\Omega + \int_{\Omega} y_i \delta \beta_i d\Omega + \int_{\Gamma^t} t_i \delta u_i dS + \int_{\Gamma^q} q_i \delta \beta_i dS - \int_{\Omega} \lambda_i (\theta_i - \beta_i) d\Omega \end{aligned} \quad (12)$$

Controlling the evolution of s is:

$$s \left(\alpha_{ijij} D_{ijkl} \alpha_{ijkl} + \kappa_{ij} \chi_{ij} \right) - 2K_c l_0 |\nabla s| + K_c \frac{(s-1)}{2l_0} = 0 \quad (13)$$

The weak form of s is produced.

$$\int_{\Omega} K_c \frac{(s-1)}{2l_0} \delta s d\Omega + 2 \int_{\Omega} K_c l_0 \nabla s \delta \nabla s d\Omega + \int_{\Omega} s \alpha_{ijij} D_{ijkl} \alpha_{ijkl} \delta s d\Omega + \int_{\Omega} s \kappa_{ij} \chi_{ij} \delta s d\Omega = 0 \quad (14)$$

It is possible to discretize the field associated with each independent variable as follows:

$$\boldsymbol{\theta} = \mathbf{H}_{\theta} \bar{\boldsymbol{\theta}}; \quad \mathbf{u} = \mathbf{H}_u \bar{\mathbf{u}}; \quad \boldsymbol{\lambda} = \mathbf{H}_{\lambda} \bar{\boldsymbol{\lambda}}; \quad s = \mathbf{H}_s \bar{s} \quad (15)$$

This work employs a three-node element with shape functions outlined in [39]. Specifically, H_θ is a linear interpolation function: $H_\theta = a_0 + a_1x + a_2y$, where the coefficients a_i are determined from the element node coordinates. H_u is a quadratic interpolation function: $H_u = b_0 + b_1x + b_2y + b_3x^2 + b_4xy + b_5y^2$; where the coefficients a_i and b_i are determined from the element node coordinates. H_s is the same linear interpolation as H_θ . H_λ is a zero-order interpolation function, in which, $H_\lambda = 1$ for points within the element and $H_\lambda = 0$ for points outside the element.

$$\boldsymbol{\kappa} = \begin{Bmatrix} \kappa_{13} \\ \kappa_{23} \end{Bmatrix} = (2\mu l^2) \boldsymbol{\chi} = (2\mu l^2) \begin{Bmatrix} \chi_{13} \\ \chi_{23} \end{Bmatrix} = (2\mu l^2) \frac{1}{2} \left\{ \frac{\partial}{\partial x}, \frac{\partial}{\partial y} \right\}^T \boldsymbol{\theta} = (2\mu l^2) \mathbf{B}_\theta \bar{\boldsymbol{\theta}} \quad (16a)$$

$$\boldsymbol{\alpha} = \begin{Bmatrix} \alpha_{11} \\ \alpha_{22} \\ 2\alpha_{12} \end{Bmatrix} = \begin{Bmatrix} u_{x,x}, 0 \\ 0, u_{y,y} \\ u_{y,x}, u_{y,x} \end{Bmatrix} = \mathbf{B}_u \bar{\mathbf{u}}, \boldsymbol{\beta} = \{\beta_{13} \beta_{23}\} = \frac{1}{2} \begin{bmatrix} -\frac{\partial}{\partial y} & \frac{\partial}{\partial x} \end{bmatrix} \begin{Bmatrix} u_x \\ u_y \end{Bmatrix} = \mathbf{B}_\beta \bar{\mathbf{u}} \quad (16b)$$

$$\alpha_{11} = \begin{bmatrix} \frac{\partial}{\partial x} & 0 \end{bmatrix} \begin{Bmatrix} u_x \\ u_y \end{Bmatrix} = \mathbf{B}_{11} \bar{\mathbf{u}}; \alpha_{22} = \begin{bmatrix} 0 & \frac{\partial}{\partial y} \end{bmatrix} \begin{Bmatrix} u_x \\ u_y \end{Bmatrix} = \mathbf{B}_{22} \bar{\mathbf{u}}; \alpha_{12} = \begin{bmatrix} \frac{\partial}{\partial y} & \frac{\partial}{\partial x} \end{bmatrix} \begin{Bmatrix} u_x \\ u_y \end{Bmatrix} = \mathbf{B}_{12} \bar{\mathbf{u}} \quad (16c)$$

$$\int_\Omega \bar{\mathbf{s}}^T \mathbf{H}_s^T \mathbf{H}_s \bar{\mathbf{s}} \bar{\mathbf{u}}^T \mathbf{B}_u^T \mathbf{D} (\mathbf{B}_u \delta \bar{\mathbf{u}}) d\Omega + \int_\Omega \bar{\mathbf{s}}^T \mathbf{H}_s^T \mathbf{H}_s \bar{\mathbf{s}} (2\mu l^2) \bar{\boldsymbol{\theta}}^T \mathbf{B}_\theta^T (\mathbf{B}_\theta \delta \bar{\boldsymbol{\theta}}) d\Omega$$

$$= \int_\Omega \delta \bar{\mathbf{u}}^T \mathbf{H}_u^T \mathbf{f} d\Omega + \int_\Omega \delta \boldsymbol{\beta}^T \mathbf{H}_\beta^T \mathbf{y} d\Omega + \int_{\Gamma^t} \delta \bar{\mathbf{u}}^T \mathbf{H}_u^T \mathbf{t} d\Gamma \quad (17)$$

$$+ \int_{\Gamma^q} \delta \boldsymbol{\beta}^T \mathbf{H}_\beta^T \mathbf{q} d\Gamma - \int_\Omega \delta \bar{\boldsymbol{\lambda}} \mathbf{H}_\lambda^T (\mathbf{H}_\theta \bar{\boldsymbol{\theta}} - \mathbf{B}_\beta \bar{\mathbf{u}}) d\Omega$$

$$\int_\Omega K_c \frac{(\bar{\mathbf{s}}^T \mathbf{H}_s^T - 1)}{2l_0} \mathbf{H}_s \delta \bar{\mathbf{s}} d\Omega + 2 \int_\Omega K_c l_0 \nabla (\bar{\mathbf{s}}^T \mathbf{H}_s^T) \nabla (\mathbf{H}_s \delta \bar{\mathbf{s}}) d\Omega \quad (18)$$

$$+ \int_\Omega \bar{\mathbf{s}}^T \mathbf{H}_s^T (\bar{\mathbf{u}}^T \mathbf{B}_u^T \mathbf{D} \mathbf{B}_u \bar{\mathbf{u}}) \mathbf{H}_s \delta \bar{\mathbf{s}} d\Omega + \int_\Omega \bar{\mathbf{s}}^T \mathbf{H}_s^T (2\mu l^2) \bar{\boldsymbol{\theta}}^T \mathbf{B}_\theta^T \mathbf{B}_\theta \bar{\boldsymbol{\theta}} \mathbf{H}_s \delta \bar{\mathbf{s}} d\Omega = 0$$

Equation (18) does not differentiate between fracture responses in tension and pressure when describing fractures. Nonetheless, there will be instances of fracture patterns that are unrealistic when the material is subjected to compression. A revised regularized concept that uses an additive decomposition of the elastic energy density E_m into volumetric and deviatoric contributions is used in preventing situations like these and, in addition, to interfere with the interpenetration of the crack faces when the material is subjected to compression. Therefore,

$E_m = E_m^+ + E_m^-$, in which:

$$E_m^+ = \frac{1}{2} K_L \langle \text{tr}(\boldsymbol{\alpha}) \rangle_+^2 + L_a (\boldsymbol{\alpha} : \boldsymbol{\alpha}) = \frac{1}{2} K_L (\alpha_{11} + \alpha_{22})_+^2 + L_a \left\{ \frac{1}{2} (\alpha_{11} - \alpha_{22})^2 + \frac{1}{2} \varepsilon_{12}^2 \right\} + \alpha \left\{ (2\mu l^2) \{ \chi_{13} \chi_{23} \} \begin{Bmatrix} \chi_{13} \\ \chi_{23} \end{Bmatrix} \right\}$$

$$= \frac{1}{2} K_L (\mathbf{B}_{11} \bar{\mathbf{u}} + \mathbf{B}_{22} \bar{\mathbf{u}})_+^2 + L_a \left\{ \frac{1}{2} (\mathbf{B}_{11} \bar{\mathbf{u}} - \mathbf{B}_{22} \bar{\mathbf{u}})^2 + \frac{1}{2} (\mathbf{B}_{12} \bar{\mathbf{u}})^2 \right\} + L_a \left\{ (2\mu l^2) (\mathbf{B}_\theta \bar{\boldsymbol{\theta}})^T \mathbf{B}_\theta \bar{\boldsymbol{\theta}} \right\} \quad (19)$$

$$E_m^- = \frac{1}{2} K_L \langle \text{tr}(\boldsymbol{\alpha}) \rangle_-^2 = \frac{1}{2} K_L (\alpha_{11} + \alpha_{22})_-^2$$

with K_L and L_a are Lamé factors,

$$\left\langle \text{tr}(\alpha_{11} + \alpha_{22}) \right\rangle_{\pm} = (\alpha_{11} + \alpha_{22})_{\pm} = \frac{1}{2} \left\{ (\alpha_{11} + \alpha_{22}) \pm |(\alpha_{11} + \alpha_{22})| \right\}.$$

The energy functional Eq. (18) has now been substituted with

$$\begin{aligned} & \int_{\Omega} K_c \frac{(\bar{s}^T \mathbf{H}_s^T - 1)}{2l_0} \mathbf{H}_s \delta \bar{s} d\Omega + 2 \int_{\Omega} K_c l_0 \nabla (\bar{s}^T \mathbf{H}_s^T) \nabla (\mathbf{H}_s \delta \bar{s}) d\Omega \\ & + \int_{\Omega} \bar{s}^T \mathbf{H}_s^T (E_m^+) \mathbf{H}_s \delta \bar{s} d\Omega + \int_{\Omega} E_m^- d\Omega = 0 \end{aligned} \quad (20)$$

In order to solve Eqs. (17, 20), the following algorithm will be used at each step of the applied load (see Algorithm 1):

Algorithm 1: Algorithm with irregular iterations

Input: initialize variable i to 0 and load the solution (\mathbf{u}_n, s_n) from step n together with the boundary constraints from the most recent step $n+1$.

$$\text{set } (\mathbf{u}^0, s^0) := (\mathbf{u}_n, s_n)$$

While crack length < plate length **do**

$$i \rightarrow i + 1$$

+ Solving Eq. (16) will provide u_1 and u_2 , from which the parts λ and ω may be determined.

+ Calculating the energy as Eq. (19).

+ Solving Eq. (19) yields the parameter s_{n+1} , which is then compared to the original variable s^0 , if $\int_{\Omega} (s_n - s^0)^2 d\Omega \leq \xi_0$

end

$$(\mathbf{u}_{n+1}, s_{n+1}) \rightarrow (\mathbf{u}^i, s^i)$$

output: $(\mathbf{u}_{n+1}, s_{n+1})$.

4. NUMERICAL RESULTS

4.1. Verification example

First, this work evaluates the reliability of the computational theory, the plate model, as shown in Figure 1. The geometry parameters of the model are prescribed as $a = b = 1\text{mm}$, $d = a/2$, and $R = l_0$. Material properties are given as $E = 210\text{GPa}$, $\nu = 0.3$, $K_c = 2700\text{N/m}$, and $l_0 = 10^{-6}\text{m}$. The results of calculating the crack growth at two different times with the results in the document [40] are shown in Figure 2 (2.a. [40]: $u_1 = 0.012\text{ mm}$; 2.b. This work: $u_1 = 0.012\text{ mm}$; 2.c. [40]: $u_1 = 0.015\text{ mm}$; 2.d. This work: $u_1 = 0.015\text{ mm}$), from which it is easy to see the reliability of the calculation theory. It should be noted in the model that: mix-mode is a crack pattern that develops as the upper surface moves along the Ox axis. On the other hand, if the underside is fixed, the crack will not develop in a path parallel to the Ox axis. It is worth noticing that this work uses a mesh with 20,000 elements, which is utilized to calculate the results below.

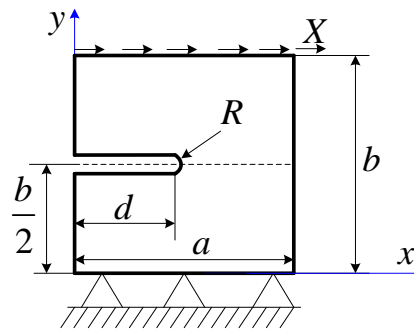


Figure 1. A computational model for crack propagation.

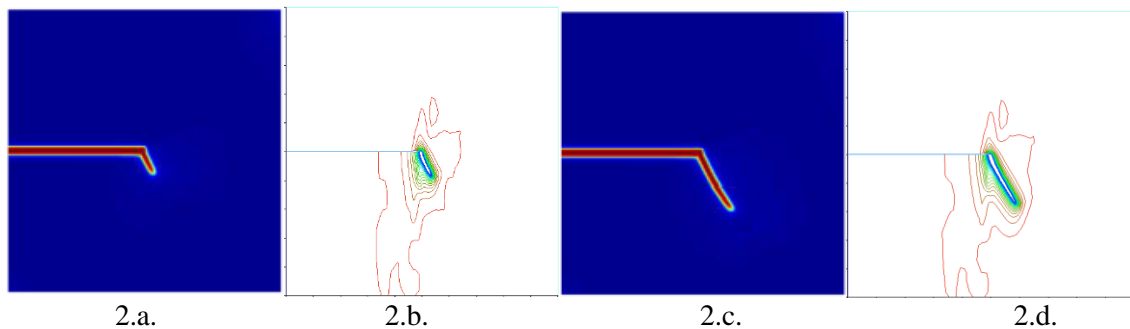


Figure 2. Crack propagation at two different time points.

4.2. The example for the case based on MCST and the case of ignoring the effect of the parameter l

To demonstrate the efficiency of the proposed formulations on crack propagation, a computational model, as shown in Fig. 1 is investigated. Material properties are given as $E = 118$ GPa, $K_c = 2,000$ N/m, $\nu = 0.26$, and $l_0 = 10^{-6}$ m. The model is subjected to the traction force τ_x in the direction x .

Computational results are presented based on the parameter l whose values range from $l = 0.002 \mu\text{m}$ to $l = 400 \mu\text{m}$. At such a small value as $l = 0.002 \mu\text{m}$, the size effect can be neglected to avoid the degradation of matrices. The size effect should be considered when the parameter l rises (i.e., $l = 400 \mu\text{m}$), thus, the results are obtained based on the MCST.

Figure 3 demonstrates the relation between the traction force (τ_x) and traction surface displacement (X) in the direction x , which corresponds to three values of parameter l . In all three cases, the traction forces are linearly dependent on the traction surface displacements until reaching the maximums, at which cracks initiate. After that, the cracks propagate rapidly, leading to a quick degradation of the traction forces. In the crack propagation stage, the results obtained from the conventional couple stress theory (i.e., $l = 0.002 \mu\text{m}$ and $l = 50 \mu\text{m}$) indicate softening behaviors, while the results obtained from the modified couple stress theory show brittle fracture characteristics.

Besides, Figure 3 shows that the higher the value of parameter l , the higher the peak traction force required for the initiation of cracks, in other words, a higher fracture energy is

required. This phenomenon can be explained as the energy in this couple stress theory consists of the elastic deformation energy evaluated based on the classic theory (CST) (i.e., size effects are neglected) and the deformation energy caused by the rotation mechanisms. Thus, stresses at crack tips evaluated based on the conventional theory are lower than those in the modified hypothesis.

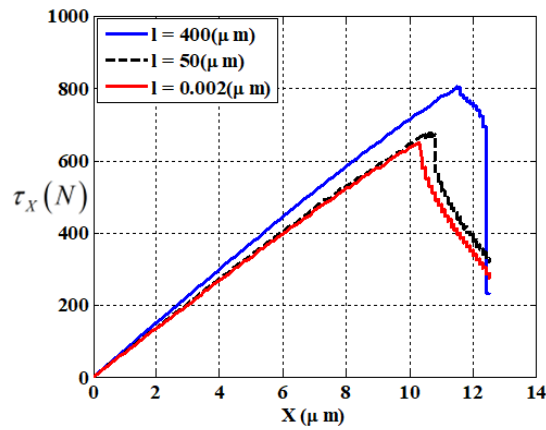


Figure 3. Relation between traction force (τ_X) and traction surface displacement (X).

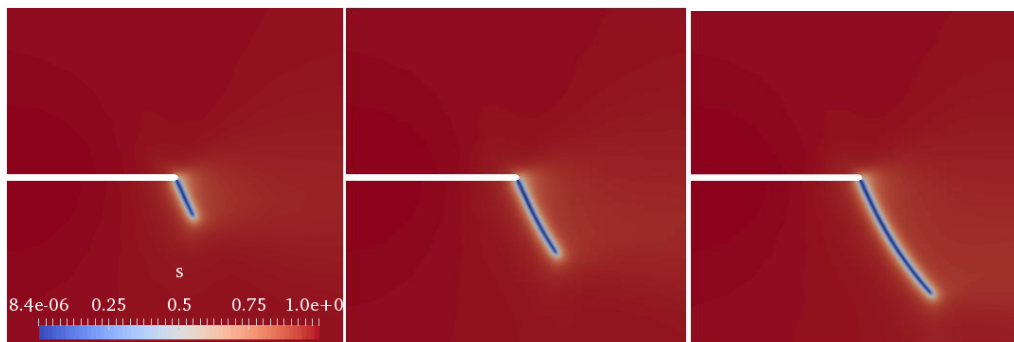


Figure 4. Phase-field variable s at locations $X = 3.04 \mu\text{m}$, $5.80 \mu\text{m}$, and $6.94 \mu\text{m}$, $l = 0.002 \mu\text{m}$.

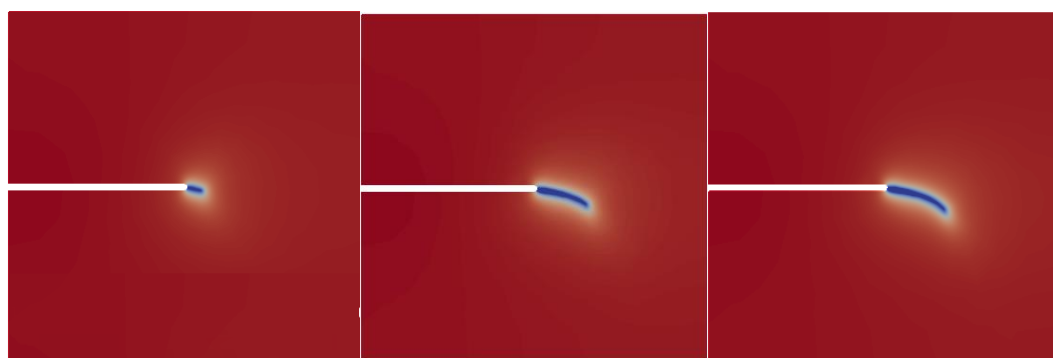


Figure 5. Phase-field variable s at locations $X = 3.04 \mu\text{m}$, $5.80 \mu\text{m}$, and $6.94 \mu\text{m}$, $l = 400 \mu\text{m}$.

Figures 4 and 5 show the change of the phase-field variable s at different stages of crack propagation, which correspond to the conventional couple stress theory (i.e., $l = 0.002 \mu\text{m}$) and the modified couple stress theory (i.e., $l = 400 \mu\text{m}$), respectively. As can be seen, the crack

propagation in Figure 5 less intense than the crack in Fig. 4, while the crack in Figure 4 appears earlier compared to the crack in Figure 5. This can be explained as follows: There is a difference in the values of parameter l and E_m^+ in Eq. (19), leading to the discrepancy result in Eq. (20). As a result, the value of the parameter s and the shape of the crack path change accordingly.

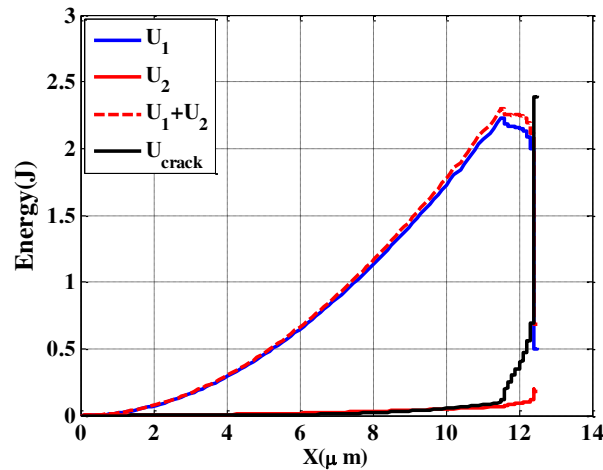


Figure 6. Relation between energy terms and traction surface displacement X with $l = 400 \mu\text{ m}$.

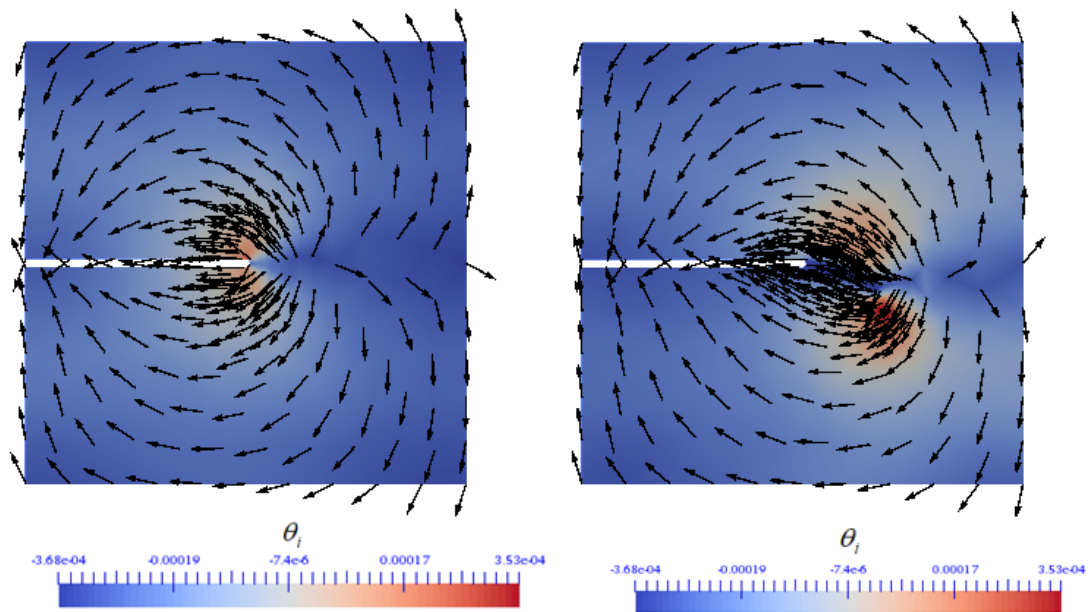


Figure 7. Change of rotation angle θ right before the initiation of cracks (left) and during the crack propagation (right), arrows indicate the couple stress vectors m , colors indicate the rotation angle field θ .

Figure 6 shows the variation of energy terms including U_1 and U_2 , U_1+U_2 , and the crack energy (i.e., U_{crack}) as defined in Eq. (11) during the propagation of cracks considering the parameter $l = 400 \mu\text{ m}$. The energy of the externally applied force is transmitted into two energy terms, U_1 and U_2 whose values increase since the application of external load. Before the initiation of cracks, the macro strain energy U_1 is predominant. After the initiation of cracks, there is a sharp increase of the crack energy U_{crack} , the macrostrain energy U_1 progressively

decreases to zero, whereas U_2 grows faster until X reaches the value of 1.24×10^{-3} m, at which point its value vanishes to zero. This location is specified as the point of a complete fracture, wherein the externally applied energy is completely transmitted into the crack energy.

Figure 7 depicts the shift in rotation angle θ just before the formation of fractures. On the top surface of the crack, the pair of stress vectors align in the x direction, indicating that the upper surface of the crack is bowed along the x -axis in the direction of the crack mouth opening. Similarly, the pair stress vectors on the surface crack are aligned along the x -axis, indicating that the under-crack surface is bowed along the x -axis in the direction of the crack mouth opening. Thus, it can be inferred that the pair stress vectors on fracture surfaces play a crucial role in the initiation of cracks along crack surfaces.

5. CONCLUSIONS

This article analyzes the crack propagation in microplates using the finite element method based on the phase-field theory and the modified couple stress theory. The obtained computational results show that the propagation characteristics of cracks in microplates are significantly different from the propagation characteristics of cracks in normal plates, where the size effects are neglected. The difference between microplates and normal plates in terms of crack initiation time, as well as crack propagation velocity, is explicitly explained due to the distribution of the energy of externally applied loads into the microstrain energy, the macrostrain energy, and crack energy. The results obtained can depict the concentration of stress at crack tips, the variation of displacement components, and phase-field variables during the propagation of cracks.

Acknowledgment. This study is funded by the Vietnam Academy of Science and Technology under grant number "VAST01.02/21-22".

CRedit authorship contribution statement: Do Van Thom: Methodology, Supervision, Writing the manuscript. Pham Hong Cong: Analysis, Solve the result number, Writing the manuscript. Doan Hong Duc: Methodology. Pham Duc Nhat: Solve the result number. Phung Van Minh, Dong Xuan Truong: Visualization

Declaration of competing interest. The authors declare that they have no known competing financial interests or personal relationships that could have appeared to influence the work reported in this paper.

REFERENCES

1. Fleck N. A., Muller G. M., Ashby M. F. and Hutchinson J. W. - Strain gradient plasticity: Theory and experiment, *Acta Metallurgica et Materialia* **42** (2) (1994) 475-487. [https://doi.org/10.1016/0956-7151\(94\)90502-9](https://doi.org/10.1016/0956-7151(94)90502-9).
2. Stölken J. S. and Evans A. G. - A microbend test method for measuring the plasticity length scale, *Acta Materialia* **46** (1998) 5109-5115. [https://doi.org/10.1016/S1359-6454\(98\)00153-0](https://doi.org/10.1016/S1359-6454(98)00153-0).
3. Stelmashenko N. A., Walls M. G., Brown L. M., and Milman Y. V. - Microindentations on W and Mo oriented single crystals: An STM study, *Acta Metallurgica et Materialia* **41** (10) (1993) 2855–2865. [https://doi.org/10.1016/0956-7151\(93\)90100-7](https://doi.org/10.1016/0956-7151(93)90100-7).
4. Nix W. D. and Gao H. - Indentation size effects in crystalline materials: A law for strain

- gradient plasticity, *Journal of the Mechanics and Physics of Solids* **46** (3) (1998) 411–425. [https://doi.org/10.1016/S0022-5096\(97\)00086-0](https://doi.org/10.1016/S0022-5096(97)00086-0).
5. Poole W. J., Ashby M. F., and Fleck N. A. - Micro-hardness of annealed and work-hardened copper polycrystals, *Scripta Materialia* **34** (4) (1996) 559-564. [https://doi.org/10.1016/1359-6462\(95\)00524-2](https://doi.org/10.1016/1359-6462(95)00524-2).
 6. Lam D. C. C., Yang F., Chong A. C. M., Wang J., and Tong P. - Experiments and theory in strain gradient elasticity, *Journal of the Mechanics and Physics of Solids* **51** (8) (2003) 1477-1508. [https://doi.org/10.1016/S0022-5096\(03\)00053-X](https://doi.org/10.1016/S0022-5096(03)00053-X).
 7. Cuenot S., Frétiigny C., Demoustier-Champagne S., and Nysten B. - Surface tension effect on the mechanical properties of nanomaterials measured by atomic force microscopy, *Physical Review B* **69** (16) (2004) 165410. <https://doi.org/10.1103/PhysRevB.69.165410>.
 8. McFarland A. W. and Colton J. S. - Role of material microstructure in plate stiffness with relevance to microcantilever sensors, *Journal of Micromechanics Microengineering* **15** (5) (2005) 1060-1067. <https://doi.org/10.1088/0960-1317/15/5/024>.
 9. Cosserat E. and Cosserat F. - Théorie des Corps déformables, *Nature* **81** (67) (1909). <https://doi.org/10.1038/081067a0>.
 10. Li X. F., Wang B. L. and Lee K. Y. - Size Effect in the Mechanical Response of Nanobeams, *Journal of Advanced Research in Mechanical Engineering* **1** (2010) 4-16.
 11. Eringen A. C. and Suhubi E. S. - Nonlinear theory of simple micro-elastic solids-I, *International Journal of Engineering Science* **2** (2) (1964) 189-203. [https://doi.org/10.1016/0020-7225\(64\)90004-7](https://doi.org/10.1016/0020-7225(64)90004-7).
 12. Eringen A. C. - On differential equations of nonlocal elasticity and solutions of screw dislocation and surface waves, *Journal of Applied Physics* **54** (9) (1983) 4703-4710. <https://doi.org/10.1063/1.332803>.
 13. Koiter W. T. - Couple Stresses in the Theory of Elasticity, I and II, *Proceedings Series B, Koninklijke Nederlandse Akademie van Wetenschappen Vol. 67, 1964*, pp. 17–44.
 14. Mindlin R. D. and Tiersten H. F. - Effects of couple-stresses in linear elasticity, *Archive for Rational Mechanics and analysis* **11** (1) (1962) 415-448. <https://doi.org/10.1007/BF00253946>.
 15. Atkinson C. and Leppington F. G. - Some calculations of the energy-release rate G for cracks in micropolar and couple-stress elastic media, *International Journal of Fracture* **10** (4) (1974) 599–602. <https://doi.org/10.1007/BF00155265>.
 16. Atkinson C. and Leppington F. G. - The effect of couple stresses on the tip of a crack, *International Journal of Solids and Structures* **13** (11) (1977) 1103-1122. [https://doi.org/10.1016/0020-7683\(77\)90080-4](https://doi.org/10.1016/0020-7683(77)90080-4).
 17. Homayounfard M. and Daneshmehr A. R. - Comments on ‘Size-dependent energy release rate formulation of notched beams based on a modified couple stress theory’ by Sherafatnia et al. [*Engng. Fract. Mech.* 116 (2014) 80-91]”, *Engineering Fracture Mechanics* **141** (2015) 120-123. <https://doi.org/10.1016/j.engfracmech.2015.04.024>.
 18. Gourgiotis P. A. and Georgiadis H. G. - An approach based on distributed dislocations and disclinations for crack problems in couple-stress elasticity, *International Journal of Solids and Structures* **45** (21) (2008) 5521-5539. <https://doi.org/10.1016/j.ijsolstr.2008.05.012>.
 19. Baxevanakis K. P. and Georgiadis H. G. - A displacement-based formulation for interaction problems between cracks and dislocation dipoles in couple-stress elasticity, *International Journal of Solids and Structures* **159** (2019) 1-20. <https://doi.org/10.1016/>

- j.ijsolstr.2018.09.015.
20. Placidi L., Misra A., and Barchiesi E. - Two-dimensional strain gradient damage modeling: a variational approach, *Zeitschrift für angewandte Mathematik und Physik* **69** (3) (2018) 56. <https://10.1007/s00033-018-0947-4>.
 21. Placidi L. and Barchiesi E. - Energy approach to brittle fracture in strain-gradient modelling, *Proceedings of the Royal Society* **474** (2210) (2018) 20170878. <https://10.1098/rspa.2017.0878>.
 22. Suh H. S., Sun W., and O'Connor D. T. - A phase field model for cohesive fracture in micropolar continua, *Computer Methods in Applied Mechanics and Engineering* **369** (2020)113181. <https://doi.org/10.1016/j.cma.2020.113181>.
 23. Thom D. V., Duc D. H., Minh P. V., and Tung N. S. - Finite Element Modelling for Free Vibration Response of Cracked Stiffened Fgm Plates, *Vietnam Journal of Science and Technology* **58** (1) (2020) 119. <https://10.15625/2525-2518/58/1/14278>.
 24. Makvandi R., Duczek S., and Juhre D. - A phase-field fracture model based on strain gradient elasticity, *Engineering Fracture Mechanics* **220** (2019) 106648. <https://doi.org/10.1016/j.engfracmech.2019.106648>.
 25. Kiendl J., Ambati M., Lorenzis L. D., Gomez H., and Reali A. - Phase-field description of brittle fracture in plates and shells, *Computer Methods in Applied Mechanics and Engineering* **312** (2016) 374-394. <https://doi.org/10.1016/j.cma.2016.09.011>.
 26. Thom D. V., Zenkour A. M., and Duc D. H. - Buckling of cracked FG plate resting on elastic foundation considering the effect of delamination phenomenon, *Composite Structures* **273** (2021) 114278. <https://doi.org/10.1016/j.compstruct.2021.114278>.
 27. Lo Y. S., Borden M. J., Ravi-Chandar K., and Landis C. M. - A phase-field model for fatigue crack growth, *Journal of the Mechanics and Physics of Solids* **132** (2019) 103684. <https://doi.org/10.1016/j.jmps.2019.103684>.
 28. Bourdin B., Francfort G. A., and Marigo J. J. - The Variational Approach to Fracture, *Journal of Elasticity* **91** (1) (2008) 5-148. <https://10.1007/s10659-007-9107-3>.
 29. Borden M. J., Verhoosel C. V., Scott M. A., Hughes T. J. R. and Landis C. M. - A phase-field description of dynamic brittle fracture, *Computer Methods in Applied Mechanics and Engineering* **217–220** (2012) 77-95. <https://doi.org/10.1016/j.cma.2012.01.008>.
 30. Do T. V., Duc D. H., Duc N. D., and Tinh B. Q. - Phase-field thermal buckling analysis for cracked functionally graded composite plates considering neutral surface, *Composite Structures* **182** (2017) 542-548. <https://doi.org/10.1016/j.compstruct.2017.09.059>.
 31. Nam V. H., Duc D. H., Khoa N. M., Thom D. V., and Hong T. T. - Phase-field buckling analysis of cracked stiffened functionally graded plates, *Composite Structures* **217** (2019) 50-59. <https://doi.org/10.1016/j.compstruct.2019.03.014>.
 32. Yang F., Chong A. C. M., Lam D. C. C., and Tong P. - Couple stress based strain gradient theory for elasticity, *International Journal of Solids and Structures* **39** (10) (2002) 2731-2743. [https://doi.org/10.1016/S0020-7683\(02\)00152-X](https://doi.org/10.1016/S0020-7683(02)00152-X).
 33. Dehrouyeh-Semnani A. M. - A discussion on different non-classical constitutive models of microbeam, *Int. J. Eng. Sci.* **85** (2014) 66-73. <https://doi.org/10.1016/j.ijengsci.2014.07.008>.
 34. Garg N. and Han C. S. - A penalty finite element approach for couple stress elasticity, *Computational Mechanics* **52** (3) (2013) 709-720. <https://10.1007/s00466-013-0842-y>.
 35. Francfort G. A. and Marigo J. J. - Revisiting brittle fracture as an energy minimization problem, *Journal of the Mechanics and Physics of Solids* **46** (8) (1998) 1319-1342.

- [https://10.1016/S0022-5096\(98\)00034-9](https://10.1016/S0022-5096(98)00034-9).
36. Miehe C., Welschinger F., and Hofacker M. - Thermodynamically consistent phase-field models of fracture: Variational principles and multi-field FE implementations, *International Journal for Numerical Methods in Engineering* **83** (10) (2010) 1273-1311. <https://10.1002/nme.2861>.
 37. Miehe C., Hofacker M., and Welschinger F. - A phase field model for rate-independent crack propagation: Robust algorithmic implementation based on operator splits, *Computer Methods in Applied Mechanics and Engineering* **199** (45–48) (2010) 2765-2778. <https://10.1016/j.cma.2010.04.011>.
 38. Sargado J. M., Keilegavlen E., Berre I., and Nordbotten J. M. - High-accuracy phase-field models for brittle fracture based on a new family of degradation functions, *Journal of the Mechanics and Physics of Solids* **111** (2018) 458-489. <https://doi.org/10.1016/j.jmps.2017.10.015>.
 39. Fish J. and Belytschko T. - *A First Course in Finite Elements*, John Wiley & Sons Ltd, 2007.
 40. Ambati M., Gerasimov T., and Lorenzis L. D. - A review on phase-field models of brittle fracture and a new fast hybrid formulation, *Computational Mechanics* **55** (2015) 383-405. <https://doi.org/10.1007/s00466-014-1109-y>.
 41. Duc H. D., Ashraf M. Z., and Do V. T. - Finite element modeling of free vibration of cracked nanoplates with flexoelectric effects, *The European Physical Journal Plus* **137** (2022) 447. <https://doi.org/10.1140/epjp/s13360-022-02631-9>.
 42. Nguyen C. T., Pham H. C., Ashraf M. Z., Duc H. D., and Phung V. M. - Finite element modeling of the bending and vibration behavior of three-layer composite plates with a crack in the core layer, *Composite Structures* **305** (2023) 116529. <https://doi.org/10.1016/j.compstruct.2022.116529>.
 43. Thom V. D., Duc H. D., Nguyen C. T. and Duc N. D. - Thermal buckling analysis of cracked functionally graded plates, *International Journal of Structural Stability and Dynamics* **22** (8) (2022) 2250089. <https://doi.org/10.1142/S0219455422500894>.
 44. Cong P. H., Duc D. H., and Thom D. V.- Phase field model for fracture based on modified couple stress, *Engineering Fracture Mechanics* **269**, (2022) 108534. <https://doi.org/10.1016/j.engfracmech.2022.108534>.
 45. Duc D. H., Thom D. V., and Phuc P. M. - Buckling analysis of variable thickness cracked nanoplates considering the flexoelectric effect, *Transport and Communications Science Journal* **73** (5) (2022) 470-485. <https://doi.org/10.47869/tcsj.73.5.3>.
 46. Duc N. D., Truong T. D., Thom D. V., and Duc D. H. - On the buckling behavior of multi-cracked FGM plates, *Proceedings of the International Conference on Advances in Computational Mechanics*, 2017, pp. 29-45. <https://doi.org/10.1007/978-981-10-7149-2-3>.